ACS APPLIED MATERIALS & INTERFACES

Research Article

www.acsami.org

Mercury Vapor Sorption and Amalgamation with a Thin Gold Film

Tingting Hou,[†] Miao Chen,[‡] George W. Greene,[†] and Roger G. Horn*[,†]

[†]Institute of Frontier Materials, Deakin University, Burwood, Victoria 3125, Australia

[‡]CSIRO Mineral Resources Flagship, Clayton, Victoria 3168, Australia

ABSTRACT: Understanding the amalgamation mechanisms between mercury and gold is of fundamental interest and importance to many mercury sensing applications. However, there is only limited and piecemeal discussion in the literature of the mechanisms by which Au−Hg amalgams are formed on thin Au films. Here, we present a comprehensive description of a series of morphological changes occurring in a thin polycrystalline Au film during Au−Hg amalgamation investigated by scanning electron microscopy (SEM), energy-dispersive X-ray spectroscopy (EDX), and atomic force microscopy (AFM). These microscopic investigations enable us to offer a coherent explanation for the features and the mechanisms of amalgamation of Hg with Au in the film. We also use an optical technique (fringes of equal chromatic order, FECO) to observe changes in optical thickness and reflectivity of the film. Amalgamation reactions in the film render it inhomogeneous, thus making optical techniques unsuitable as a method for quantitative monitoring of Hg vapor using Au films of this type.

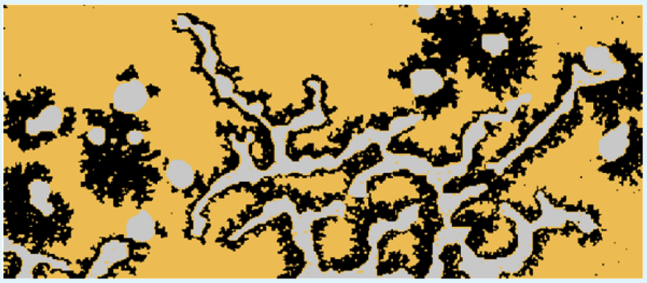

KEYWORDS: *Thin gold film, mercury, mercury sorption, mercury sensor, amalgamation mechanism*

1. INTRODUCTION

Mercury is a well-known hazardous contaminant that is frequently present in elemental (Hg^0, gaseous), inorganic (Hg^+ and Hg^{2+}) and organic (methylmercury and ethylmercury) forms in the environment. This pollutant, mostly from power plants, combustion of fossil fuels, mining ore processing and solid waste incineration, can cause serious damage to human organs and immune systems from chronic exposure even at low level.[1] Elemental mercury is the dominant species in the atmosphere due to its long residence time (0.5−2 years) and long distance migration (tens of thousands of kilometres).[2] In some circumstances, elemental mercury can be converted to the inorganic or organic species, both of which are highly toxic and can bioaccumulate in the aquatic food chain.[3] With the growing awareness of its adverse effects on human health and the ecosystem, it is important to develop sensitive and selective methods to quantify atmospheric mercury.

There are a number of well-established techniques that have been developed to detect gaseous Hg in air and flue gas. Gold (Au) is a well-known mercury sorbent due to the strong affinity and specificity between Hg and Au, with easy release of Hg load by heating or dissolution. Traditionally, a gold trap (typically bulk metal in the form of foil, wire or mesh, or thin film prepared on glass tubes or spheres) is used to capture and preconcentrate Hg vapor, followed by quantitative analysis of the sorbed Hg using one of two different methods. One is based on thermal desorption and gas-phase determination, in which the sorbed Hg is released into an argon carrier stream by heating and then is quantified by gas phase spectroscopic techniques, such as cold vapor atomic fluorescence spectroscopy (CVAFS)[4] or cold vapor atomic absorption spectroscopy (CVAAS).[5] The other method is based on acidic dissolution, in which mercury is dissolved from the substrate in strong acid solution and its amount in the solution is subsequently determined using an ion-analysis technology such as inductively coupled plasma-atomic emission spectrometry (ICP-AES).[6] Although these techniques have been proven to have excellent performance, time-consuming sample preconcentration and sophisticated equipment limit their practical application in the field. In addition, volatile or dissolution loss, condensation of water vapor on the tubing, and spectral interferences from organics are common problems leading to irreproducibility and loss of sensitivity.[7]

To overcome these limitations, several other techniques using thin Au film-based electric-, optical-, and mass-sensitive sensors have been suggested for Hg vapor detection. Here, the Au film acts not only as a strong mercury sorbent, but also functions as a transducer. For instance, McNernery et al. demonstrated that the electrical resistance change of an Au film is proportional to Hg sorption from nanogram to microgram levels.[8] Hg has also been detected by monitoring the accumulated mass using a quartz crystal microbalance (QCM).[9,10] In addition, some optical techniques such as optical reflectometry,[11] spectroscopic ellipsometry,[12] and surface plasmon resonance spectroscopy (SPR)[12,13] have been used to study the Hg sorption on thin gold films. With the development of nanotechnology in recent years, a few novel sensors based on the plasmonic absorbance of gold nano-

Received: July 31, 2015
Accepted: September 30, 2015
Published: October 8, 2015

DOI: 10.1021/acsami.5b07002
ACS Appl. Mater. Interfaces 2015, 7, 23172−23181

particle[14−18] and nanorods[19,20] suspended in solution[15,18,19] or immobilized on functionalized substrates[14,16,17,20] have been developed to detect mercury using UV−vis absorption spectroscopy,[16,19,20] SPR,[15,21] and surface-enhanced Raman spectroscopy (SERS).[22] Although most of the gold-based mercury vapor sensors provide low detection limits and fast response times, questions remain about the reversibility, time stability, and exposure limits of these sensors.

Previous studies of Hg sorption to Au films[11,12,23−25] indicate that during an initial period (around 30 min in saturated vapor[12,23,26]) Hg is adsorbed to the surface in a submonolayer, and this adsorption is claimed to be reversible.[11] Some authors have described the surface as "saturated" after this time, although there is clear evidence that further sorption occurs, accompanied by diffusion and/or mixing of Hg below the surface of the Au film.[26] It has been shown that this diffusion occurs more readily in a polycrystalline film than in a single-crystal Au film with a (111) surface,[12,25,26] which is consistent with accumulation of Hg and/or its diffusion at grain boundaries.

Following the presumed initial adsorption of Hg atop the Au surface, there is evidence for the formation of islands[25−29] on, and pits[27] in the gold film. Although some authors have argued that the islands are accumulations of mercury atoms,[25] others have argued that they include gold atoms from the substrate which have migrated there via a place exchange mechanism in which some mercury atoms are buried below the surface.[26] Some authors have shown that following the formation of islands, dendritic structures appear;[11,23] both the islands and the dendritic structures can be of micrometer dimensions.

Apart from the place exchange mechanism that only describes island formation at the onset of the "saturated" state,[26] there is little discussion in the literature of the mechanisms by which islands form and grow, why the pits form, and why the dendritic structure appears. In the present paper, we present the first comprehensive description of the suite of morphological changes that occur in a thin polycrystalline gold film during Au−Hg amalgamation on a microscopic level. The changes have been investigated by scanning electron microscopy (SEM), energy-dispersive X-ray spectroscopy (EDX), and atomic force microscopy (AFM). We also use an optical technique (fringes of equal chromatic order, FECO) to observe changes in the film's optical thickness and reflectivity on exposure to mercury. The changes in optical properties are difficult to model because the amalgamation process renders the film inhomogeneous and strongly scattering, which serves to demonstrate the inutility of this or related optical methods for quantitative sensing.

2. MATERIALS AND METHODS

2.1. Materials. Silicon wafers, 4" (100 mm) in diameter, with a 5 μm thick thermally grown oxide (SiO_2) layer were purchased from SWI Semiconductor Wafer Inc., Taiwan. Elemental mercury (Hg, electronic grade, 99.999%, Aldrich) was purchased from Sigma-Aldrich Pty. Ltd. (Australia). Anhydrous ethanol (C_2H_5OH, 99.5%, denatured, Fisher Scientific), sulfuric acid (H_2SO_4, 98%) and hydrogen peroxide (H_2O_2, 32%) were analytical grade reagents purchased from ASIS Scientific Pty Ltd. (Australia) and used as received without further purification. The water (H_2O) used in this work was taken from a Millipore Milli-Q ultrapure water purification system.

2.2. Preparation of Thin Gold Films. Thermally oxidized Si wafers were used as a substrate. Prior to use, the wafers were cut into 1 cm × 1 cm chips and were cleaned using "piranha solution" consisting of 98% H_2SO_4 and 30% H_2O_2 (v/v = 7:3) at 80 °C for 1 h. (*Note that piranha solution must be handled with care: it is strongly oxidizing and reacts violently with organics*). Finally, the substrates were thoroughly rinsed with Milli-Q water and dried with nitrogen gas. Thin gold films for mercury sorption were prepared by e-beam evaporation of gold (99.99% purity, AGS Metals Pty Ltd.) onto cleaned thermal oxide Si wafer at a rate of 0.2 nm/s using an Intlvac Nanochrome II Electron Beam Evaporator (Melbourne Centre for Nanofabrication, MCN) at a base pressure of 7×10^{-6} Torr. For some experiments the gold evaporation was preceded by e-beam evaporation of a very thin (2 nm) layer of chromium to promote adhesion of gold to the substrate. The thickness of the deposited gold film (20 nm) was monitored by an inbuilt QCM. For half−half patterned Au films used in some experiments, each piece of Si wafer was covered by a mask that only allowed half the surface to be exposed to the gold evaporation beam.

The freshly prepared Au substrates were stored in a vacuum desiccator and exposed to mercury vapor within a few days of preparation. No differences were observed between substrates that were used immediately after preparation and those used a few days later.

2.3. Mercury Vapor Exposure. The Au film samples were exposed to mercury by placing them in a small capped glass jar (volume 280 mL) with several mercury droplets (~0.3 g) also in the jar. Because of its high volatility, Hg vapor soon reached its saturated concentration in the jar. The mercury exposure time was the time spent by the Au-coated wafer in the sealed jar.

2.4. Microscopic Characterization. Films were examined for morphological changes by SEM prior to and after mercury exposure. SEM images were captured with a Zeiss Gemini Supra 55 VP instrument. For imaging, working distances were typically around 5 mm and emission voltages were set to 20 kV. For EDX measurements, the working distance was fixed at 10 mm and the emission voltage was 5 kV for gold and mercury. Samples were attached to an aluminum stub with conductive silver paint.

To provide three-dimensional information on the Au−Hg amalgamation process, we imaged surfaces in tapping mode in air using a Veeco Dimension Icon AFM. The cantilevers (MPP-11220−10 with a nominal 40 nm sharp tip) were Bruker RTESPA model tapping mode levers, with nominal resonant frequencies of 300 kHz and spring constants of 40 N/m, respectively. Typical scan size was 1 × 1 μm^2 with 512 × 512 sampling points. In post processing, images were "flattened" to ensure coplanarity. No further manipulations were performed.

2.5. Optical Setup and Data Acquisition. The optical thickness of the gold film before and after exposure to mercury was monitored by optical interference using the fringes of equal chromatic order (FECO) method.[30] The basic working principle of FECO is to use white light-illuminated Fabry−Perot interference occurring in thin transparent films and analyze the wavelengths that interfere constructively or destructively following reflections from the front and rear surfaces of a transparent thin film (as in the colors of soap bubbles or oil films on water). The film could be a single layer or multiple layers of different materials; in the present case, the thin film under examination is formed by the 5 μm layer of thermal oxide (silica) grown on a silicon wafer, plus the ~20 nm layer of gold or gold/mercury. Making use of an optical spectrograph (described below) an interference fringe of a particular "chromatic" order can be observed, together with any changes in its wavelength and/or intensity. In principle, any interaction occurring on the surface, including Hg vapor sorption on the Au film, can induce changes in refractive index and/or physical thickness and/or optical phase change on reflection; thus it would seem possible to use FECO technique to characterize this surface sorption behavior.

The optical setup consists of a tungsten halogen lamp (LSH-T100, 350−2400 nm), a compact sample compartment and an imaging spectrometer (Horiba Jobin Yvon model iHR 550) with CCD camera (Synapse), as shown in Figure 1. In this setup, collimated white light was directed perpendicularly onto the front surface of the Si wafer which was mounted in the sample holder. The combined reflected light from the top and buried interfaces of the SiO_2 film was focused on the entrance slit of the spectrometer, and the image at the exit slit

DOI: 10.1021/acsami.5b07002
ACS Appl. Mater. Interfaces 2015, 7, 23172−23181

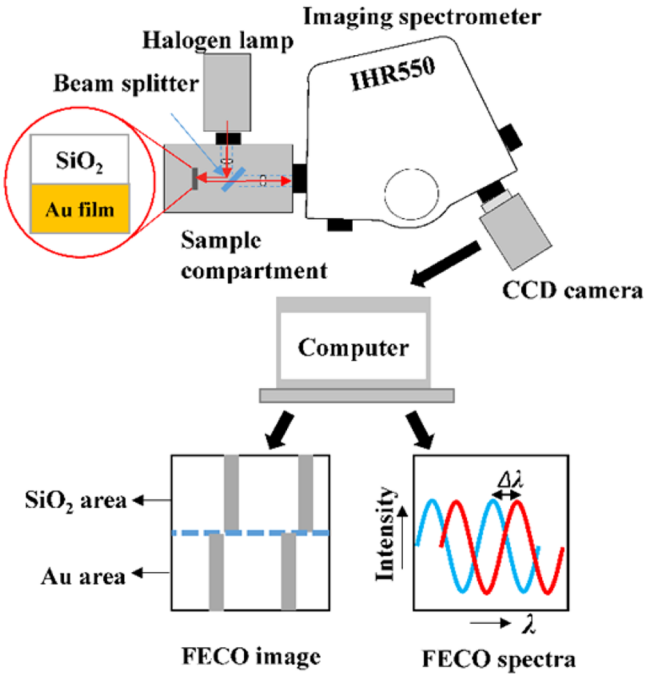

Figure 1. Schematic of FECO imaging setup. A thermally oxidized Si wafer chip (1 × 1 cm^2) has one-half coated by a 20 nm Au film. Reflection of white light from the front and rear surfaces of the SiO_2 layer results in a Fabry−Perot interference pattern. Sorption of mercury vapor on the Au film coated on the wafer induces a change in the optical thickness, giving rise to wavelength shifts in the fringe pattern that can be captured by the CCD camera, and then quantified by the instrument's software.

was recorded by the CCD camera and displayed either as an interference spectrum (intensity vs wavelength) or as an interference image (FECO fringes). Data acquisition and processing were performed by the instrument's proprietary software (SynerJY) running on a personal computer.

3. RESULTS

3.1. Morphology Characterization. Figure 2 presents SEM images of Au films, showing the morphological changes resulting from exposure to Hg vapor for increasing times. The concentration of mercury vapor was 13−17 ng/mL (15 ± 2 ppm) at 21−23 °C[31] and the exposure time ranged from 0 to 15 h. Figure 2a shows that bare Au film exhibited polycrystalline morphology with visible grain boundaries. The root-mean-square (rms) roughness is less than 3 nm, and the grain size is in the 10−30 nm range based on AFM measurement as shown in Figure 3a.

After 1 h of exposure to Hg vapor, there are some isolated protruding islands, typically 0.1−0.5 μm in diameter, appearing on the Au surface, corresponding to bright domains in secondary electron imaging mode of SEM seen at a lower magnification in Figure 2b. AFM analysis (in Figure 3b′) showed that the island size is 50−100 nm in diameter and 7−10 nm in height at this stage, which is considerably greater than the grain size of the gold film and far more than the height of an atomic monolayer. The distribution of islands is nonuniform, which suggests a random distribution of adsorption sites and/or island nucleation sites. Previous work[11,29] has suggested that Hg adsorption is favored at grain boundaries or other defects in gold films. Additionally, numerous pits have appeared on the surface, seen as dark spots in the inset to Figure 2b). These pits

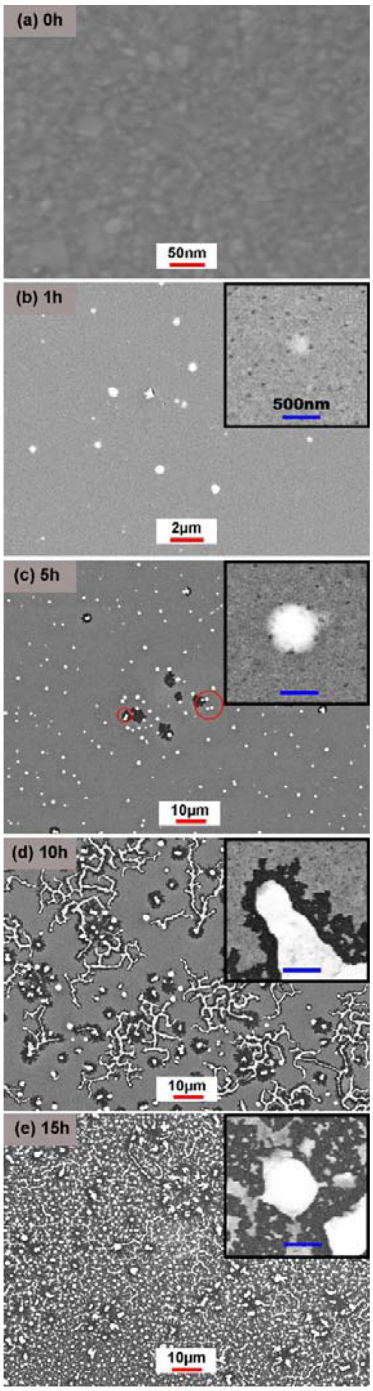

Figure 2. SEM images of Au film (a) before and (b−e) after Hg sorption at each exposure time. The scale bar in inset images represents 500 nm.

are around 10−20 nm in diameter and are spread uniformly, with a typical spacing of ∼200 nm between them. On close inspection (Figures 2b inset, 2c, and 4a), it is seen that islands are frequently decorated by pits at their edges. The depth of the pits cannot be determined by AFM because their diameter is smaller than the tip radius; thus it is not clear whether they are depressions in the film, or pinholes that go all the way through it. The formation of holes is noteworthy since it is the surface of the Au film that is exposed to adsorbing mercury atoms; the observation suggests that Hg has somehow caused relocation of Au atoms.

DOI: 10.1021/acsami.5b07002
ACS Appl. Mater. Interfaces 2015, 7, 23172−23181

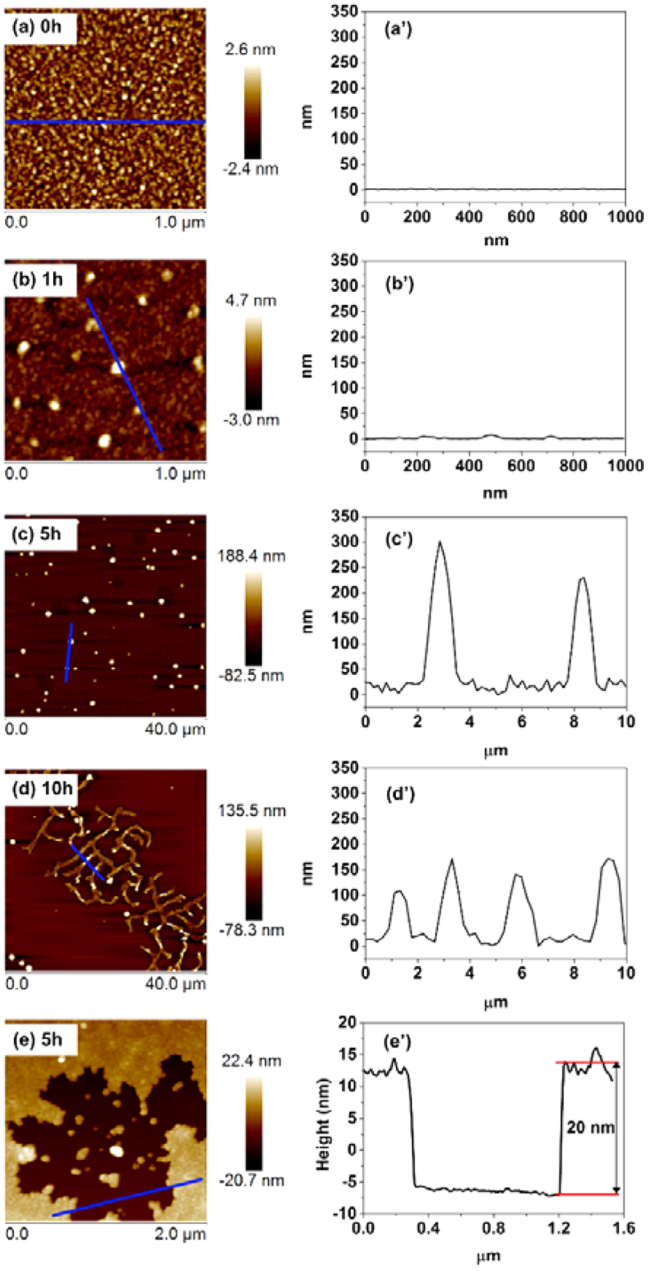

Figure 3. (a–e) AFM height images and (a′–e′) line profiles for surfaces (a, a′) before and after Hg sorption for (b, b′) 1, (c, c′) 5, and (d, d′) 10 h; note the lower magnifications in c and d. (e) One of the black voids in image c with higher magnification; (e′) section analysis showing that the step height of 20 nm between the top of the film and the bottom of the dark areas equals the Au film thickness, indicating that the Au film at this area is fully consumed.

The observed pits could possibly be artifacts of the SEM contrast mechanism due to different local conductivity over areas of different metallic composition following exposure to mercury. However, we are able to rule out this possibility because a much smaller number of pits is observed under the same conditions of mercury exposure when the gold film is prepared with a thin layer of Cr (2 nm) evaporated first to promote adhesion to the wafer (Figure 4). The presence of pits is therefore related both to Hg exposure and to the mobility of gold in the deposited film.

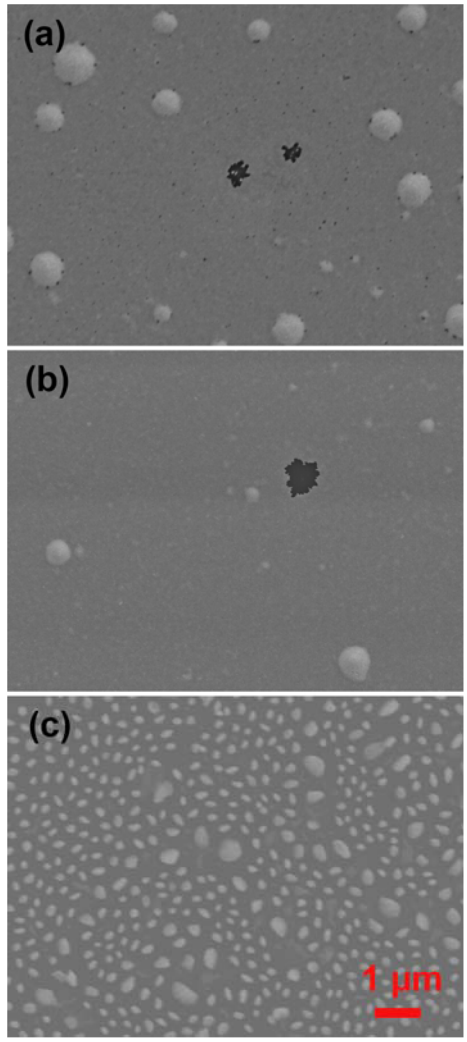

Figure 4. SEM images showing the sorption of Hg on Au film (a) without and (b) with Cr adhesion layer under the same conditions of Hg exposure (2 h). (c) After 15 h Hg exposure, the Au film with Cr adhesion layer was covered by micrometer-scale islands, though less disrupted than the film without the adhesion layer (Figure 2e).

After 5 h of exposure, the maximum island size has grown to about 1 μm, while their density (the number per unit area) has increased significantly (Figure 2c). AFM analysis shows that the typical island height has also increased, to about 300 nm (Figure 3c′). Furthermore, we see islands begin to join together, with a few doublets appearing (some examples are marked with red circles). It is noteworthy that the islands remain circular even when joined as doublets—rather than coalesce there appears to be an upper limit to the diameter of individual islands. This image also reveals the appearance of a new feature—black areas corresponding to voids in the gold film, with areas much larger than the pits discussed above.

Further information on changes in the film is provided by EDX analysis in Figure 5. Figure 5b shows that the islands contain Au and Hg (with trace amounts of Si and O also detected), which would be expected if the islands consisted of Au–Hg amalgam. Figure 5c demonstrates that the Au film in the black areas appears to have been fully consumed by Hg and the underlying SiO_2 is exposed. There is further evidence from AFM section analysis (Figure 3e′), in which the step height of 20 nm between the top of the film and the bottom of the black

DOI: 10.1021/acsami.5b07002
ACS Appl. Mater. Interfaces 2015, 7, 23172–23181

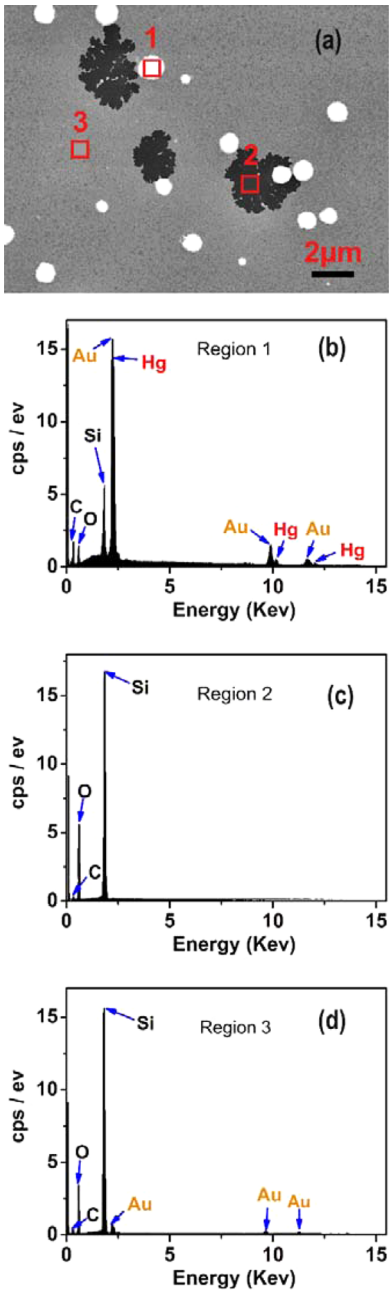

Figure 5. (a) Surface morphology of Au film after exposure to Hg vapor for 5 h; (b) EDX of spot 1 on a white island; (c) EDX of spot 2 on a black void; and (d) EDX of spot 3 on Au coated areas. Si and O from the substrate show up in all images because the penetration depth exceeds the thickness of the film.

areas equals the Au film thickness. Furthermore, the black areas are generally associated with island doublets or a higher than average number of islands in the vicinity.

After 10 h of exposure (Figure 2d), most of the islands have grown into long fingers 1−2 μm in width, with the fingers connected in dendritic formations. The height of the fingers remains comparable (100−150 nm) to the height of the islands (Figure 3d′). Each finger is surrounded by a black "moat" where the gold film has been consumed. It appears that gold from the film has migrated into nearby islands and/or fingers of mercury-rich material that is thicker (hence brighter in SEM images) than the original film. Previous authors[11,32] have reported similar dendritic structures developing, but with little discussion of the reasons for their formation.

Eventually after 15 h, most or all of the Au from the film has been drawn into Hg-rich dendrites and/or islands (see Figure 2e). Many of the dendrites have broken up into isolated islands, though a few remain. At this point, the original continuous Au film has been completely disrupted by the Hg vapor to leave a discontinuous distribution of amalgam.

It must be stressed that it is not possible to use SEM (or AFM) to analyze the morphology changes at the exactly same location after repeated exposure of Au film to Hg vapor. Thus, the differences between images in Figures 2 and 5 could be attributed to surface heterogeneity as well as the different exposure time. However, the essential morphological features are always seen in images taken from various areas of the same sample, and there is less variation in the details upon increased exposure time.

3.2. FECO Measurement and Interpretation. To observe the FECO response to Hg sorption on an Au film, an experiment was conducted as illustrated in Figure 1. Half the surface of a Si wafer chip with a thermally oxidized SiO_2 layer was coated with a gold film of thickness approximately 20 nm (Figure 6a). Here, the bare SiO_2 domain acts as an inbuilt reference; we assume that the FECO fringes in this domain would not change on exposure to mercury vapor because no interaction is expected between Hg and SiO_2. As shown in Figure 6a′, the reflection FECO fringes have the appearance of a series of dark vertical stripes on a bright background along the wavelength scale, which are due to the destructive interference of light reflected from the top (SiO_2-air or SiO_2−Au) and buried (SiO_2−Si) interfaces. The dark fringes appear clearer and sharper in the gold-coated region than in the uncoated half of the sample because of the higher reflectivity of the former.

Figure 6a−e shows the optical microscopic images of the Au film before and after various exposure times to Hg vapor. It is apparent that after 1 h or more of exposure the mercury causes damage to the film, initially in the form of small spots appearing, which grow larger and more numerous until after 15 h the film is extensively damaged and inhomogeneous. This observation is not in agreement with some previous studies arguing that the Hg adsorption is limited to the surface of a gold film.[26] The discrepancy in observations may result from morphological properties of the Au film used for mercury collection, such as polycrystalline Au surfaces in our case and single-crystal Au (111) surfaces in the previous studies; Morris and Szulczewski have demonstrated that mercury diffuses into the film when it is polycrystalline but not when it is single crystal with the (111) orientation.[12] This is because diffusion is faster in polycrystalline materials compared to single crystals because of more rapid diffusion along grain boundaries.

Figure 6a′−e′ shows representative FECO images of half−half patterned SiO_2/Au film before and after mercury exposure. It can be seen that two changes occurred with Hg sorption. One is the intensity change between FECO fringes in SiO_2 and Au domains. As a result of Hg sorption, the contrast and the sharpness of FECO fringes in Au domains decreased significantly, particularly at exposure times greater than 5 h. Another change is in the fringe positions (wavelengths of the intensity minima) in the Au film domain, which move to shorter wavelengths as a result of the optical phase change at the interface between SiO_2 and gold.[33] However, between 10 and 15 h exposure, there is an abrupt shift back to a fringe position close to that in the bare SiO_2 domains, as shown in

DOI: 10.1021/acsami.5b07002
ACS Appl. Mater. Interfaces 2015, 7, 23172−23181

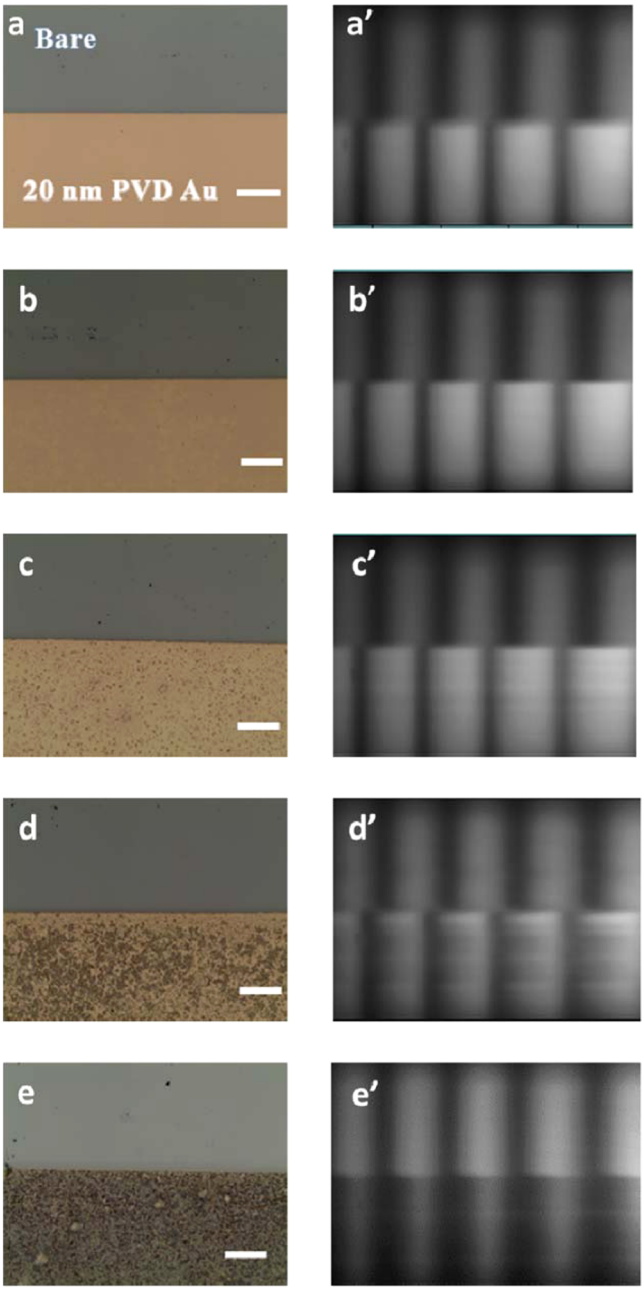

Figure 6. (a–e) Optical microscopy and (a′–e′) FECO images of Au film (a, a′) before and after mercury exposure at (b, b′) 1, (c, c′) 5, (d, d′) 10, and (e, e′) 15 h. The scale bar in optical images is 50 μm. The horizontal scale of the FECO images is wavelength, from 590 to 690 nm.

Figure 6e′. The fringe shifts for exposure times less than 10 h are more subtle, but can be seen in the spectral (intensity vs wavelength) plot (Figure 7). Spots and inhomogeneities in the Au–Hg films that are visible in the optical micrographs, Figures 2c and 2d, show up as horizontal "scratches" in Figure 6c′, d′ because they block light of all wavelengths.

The corresponding spectral curves shown in Figure 7 suggest that the effect of Hg sorption on the metal surface could be evaluated by determining the shifts of fringe position or by relating the changes in fringe intensity at a fixed fringe order. Figure 8 depicts the changes in intensity of a fringe, and the shift ($\Delta\lambda$) of a dark fringe near 632 nm during Hg exposure.

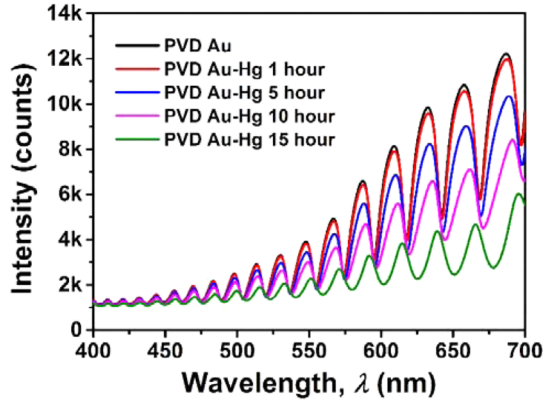

Figure 7. FECO spectra of Au films before and after mercury exposure in air for 1, 5, 10, and 15 h. The general increase in intensity with wavelength is a characteristic of the halogen lamp light source.

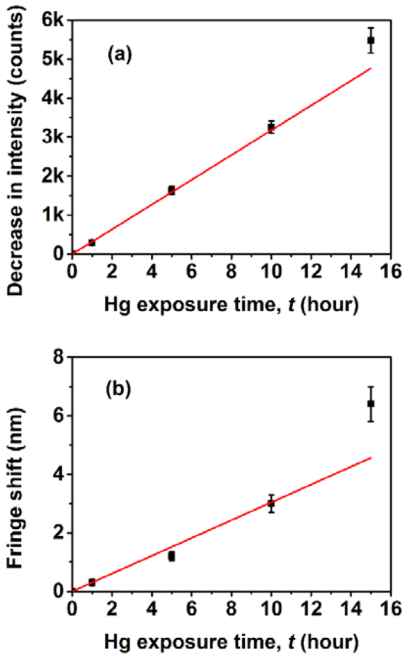

Figure 8. Changes in (a) intensity and (b) wavelength of the dark fringe near 632 nm for the first 15 h of Hg exposure.

In principle, it would be possible to match an optical model of multilayer films using appropriate optical properties[34] to the experimental data to determine an effective film thickness of adsorbed mercury. Although fringe shifts and contrast changes do occur as the result of Hg exposure, the optical micrographs as well as the sudden fringe shift between 10 and 15 h of exposure make us believe that the FECO responses result from morphological changes of the gold film as much as simply changes in optical thickness or optical phase change. The obvious inhomogeneity of the film after long exposure renders the optical modeling intractable because the latter does not include the possibility of light scattering. The same comment applies to related optical methods such as ellipsometry, SPR, or interferometry.

4. AMALGAMATION MECHANISM

Our observations reveal several steps in the adsorption of mercury on a thin gold film, all of which are consistent with previous observations in the literature. However, no previous

DOI: 10.1021/acsami.5b07002
ACS Appl. Mater. Interfaces 2015, 7, 23172–23181

papers have discussed in detail the whole sequence of features and the mechanism(s) by which they are formed. The features to be explained here are (a) the formation of pits in the gold film; (b) the formation of mercury-rich islands on top of a polycrystalline gold film, with islands frequently surrounded by pits; (c) the growth of islands to about 1 μm in diameter; (d) the coalescence/joining of islands into pairs; (e) the development of dendritic structure with neighboring bare strips in the gold film; (f) the final breakup of dendrites into a threads-plus islands structure.

4.1. Formation of Pits and Islands. Mercury adsorption-induced defect and island formation has been reported previously by Levlin's group.[26,27] This group observed pits typically 2−5 nm in diameter and 0.2−0.3 nm in depth and islands around 5−10 nm in diameter (i.e., smaller than those in the inset to Figure 2b) when they studied Hg adsorption on Au (111) films using scanning tunneling microscopy (STM).[27] The mechanism they proposed for island formation was a place exchange model,[26,35,36] in which some of the Hg atoms arriving at the Au surface transfer below the first surface layer and exchange places with top layer Au atoms. The ejected Au atoms transfer to the top of the layer and diffuse until they adsorb at a step edge or collide with other atoms forming an island. This model can successfully explain island formation for mercury adsorption on Au (111), but does not explain why the pits form. Levlin et al. conclude that the observed pits are either real vacancy clusters or clusters of foreign atoms on the surface.[27] In a later publication,[26] they observed fewer pits, and attributed this difference to the occasional pulses of high concentration mercury vapor due to a less stable mercury evaporation system in their earlier experiments.

Small pits have also been observed in gold films when thiol molecules adsorb on Au (111) surfaces to form self-assembled monolayers (SAMs).[37−39] The pits, detected by STM measurements, are comparable in size to those reported by Levlin[27] (a few nm in diameter and just 0.2−0.3 nm deep), corresponding to a single atomic layer of gold. This shows that they are formed in the gold film rather than the thiol layer.

Poirier[37] provided an explanation for the formation of pits (or "vacancy islands" in his terminology), which was later extended by Yang and Liu[39] to account for minor variations occurring with different types of adsorbed thiol. The explanation derives from consideration of reconstruction processes at noble metal surfaces and how such a reconstruction can be driven by interactions between the chemisorbed species and the underlying metal. Theoretical investigations and experimental observations have both revealed that chemisorption of adsorbates on Au surfaces can affect the electronic charge distribution within the topmost layer and/or weaken the bond between the topmost and the second layer, causing the atoms in the top surface to rearrange themselves.[40−42] This implies that a static surface structural model, one of the simplifying assumptions behind descriptions of chemical interaction between adsorbates and surfaces, must be replaced by a dynamic reconstruction model in which the surface atoms change their equilibrium positions in response to the changing chemical bonding environment imposed by the adsorption of atoms and molecules.[41] Ultrahigh-vacuum STM has also demonstrated that the reconstructions usually occur with the adsorbates being able to "pull out" metal atoms from the surface and form new structures locally.[41]

The explanation for the appearance of pits or "vacancy islands" following thiol adsorption to Au(111) is that the close packing of alkanethiol monolayers and the strong interaction between thiol and gold and causes a rearrangement of the gold atom packing in the surface layer.[37] This leads to some gold atoms being evicted from the surface, and these can readily diffuse over the surface and condense at step edges. The vacancies that are left in the top layer can also diffuse, though more slowly, and combine with each other to form vacancy islands that are the observed pits.

Drawing from the above adsorbate-induced reconstruction model, we suggest that when Hg atoms initially adsorb onto the Au film they weaken Au−Au interaction and attract gold atoms because of strong Au−Hg bonding. This would have higher probability at a defect in the gold film where the Au−Au interaction is already weaker than it is in a regular crystal lattice site. Such local perturbation following Au−Hg interaction could generate an in-plane tensile stress in the Au surface that can be released by ejection of Au atoms, creating mobile adatoms on, and atomic vacancies in, the surface layer. As the surface reaction proceeds, atomic vacancies would nucleate and coalesce to form microscopic voids in domains not covered by Hg, while the ejected Au atoms would migrate rapidly and combine with Hg to form mercury-rich islands, which appear within 1 h of Hg exposure (Figure 2b, c). The mobilities of adatoms and atomic vacancies depend on temperature, adsorbate concentration and coverage. According to previous literature adatoms have much smaller energy barriers (E_d = 0.102 eV) for diffusion than vacancies (E_d = 0.455 eV) in the case of Au (111) film.[39,43] Slower diffusion of vacancies than adatoms leads to formation of pits that are much smaller than the islands, with an areal density greater for pits than islands. This accounts for the experimental observations of initial pit and island formation on Au surfaces.

Evidently as the sorption process continues, the Hg atoms that arrive at the surface condense in the islands (Figure 5) rather than forming uniform monolayers or multilayers on the gold surface, perhaps because the island edges provide favorable adsorption sites. We propose that the islands are a nascent amalgam whose composition would equilibrate at a fixed stoichiometry. There is a lack of agreement in the literature about the composition of stable amalgam phases, with Rolfe and Hume−Rothery[44] identifying Au_3Hg and Au_2Hg in their determination of the Au−Hg phase diagram and claiming that there is no more mercury-rich phase present, while acknowledging that this is in contradiction to previous findings. Butler[11] uses X-ray fluorescence spectroscopy to identify an amalgam composition of approximately Au_2Hg_3 following exposure of a thin gold film to mercury vapor, while Kita and Kon[45] give evidence for a $AuHg_2$ phase. With the small volume of amalgam present in islands observed in the present experiments, we have not been able to use X-ray diffraction (XRD) to measure the Au−Hg ratio nor crystal structure to identify a particular amalgam composition, and the overlapping Au and Hg peaks in EDX (Figure 5b) prevent quantitation by this method. The islands, even at their maximum size of ∼1 μm, are too small to be resolved in X-ray photoelectron spectroscopy (XPS) analysis.

Our proposal is that as fresh mercury atoms accumulate in the islands, gold atoms also diffuse there to approach or maintain an equilibrium composition of the amalgam. Such a driving force to pull Au out of the film and into the amalgam islands is an essential component of our explanation for all the observed changes in film morphology.

DOI: 10.1021/acsami.5b07002
ACS Appl. Mater. Interfaces 2015, 7, 23172−23181

It is evident in the present experiments that pits in the Au film grow larger than those reported by Levlin, up to 100 nm in diameter and much more than one atomic layer in depth. It is seen in Figure 2c,d and discussed further below that the pits adjacent to mercury-rich islands eventually grow to the entire depth of the film (20 nm), leaving voids in the film. To explain such a phenomenon requires Au atoms in the film to be continually drawn into the mercury-rich islands during ongoing exposure to mercury vapor.

The appearance of pits implies that Au is mobile during Hg adsorption and is being drawn to the mercury-rich islands, rather than islands moving around the surface and mopping up gold atoms. Further evidence comes from an experiment in which Cr was used as an adhesion layer for the gold film, so the Au would not diffuse so readily. The results (Figure 4b) show no small pits and fewer islands forming in the Au film under the same conditions of Hg exposure.

4.2. Growth of Mercury-Rich Islands. Chen and Washburn[46] offer an explanation for a transition from flat quasi-2D platelets like those observed in Figures 2b, 3b, and 3b′ to thicker dome-shaped islands as seen in (Figures 2c, 3c, and 3c′) and reported by Nowakowksi.[29] Their explanation is based on a consideration of elastic strain energy in heteroepitaxial film growth caused by mismatch in the lattice parameters of substrate and adsorbate, and they show that platelets grow up to a critical size, after which they thicken to domed 3D islands. The critical size depends inversely on the lattice mismatch between the substrate and epitaxial layer. Other authors[47] speak of island growth via an Ostwald ripening mechanism involving exchange of material by diffusion from small islands to larger ones. We do not have information to distinguish between these possibilities in our experiments, although in the following section, we note an argument against the Ostwald ripening mechanism.

Chen and Washburn[46] have also provided an explanation for islands growing to a certain size, after which their growth slows significantly or stops. The mismatch between atomic lattices in the island and the underlying substrate creates strain in the substrate just outside the boundary of an island. Atoms diffuse over the substrate to reach the islands and contribute to their growth, but the strain field around an island creates an energy barrier to diffusion. The magnitude of the strain, and hence the energy barrier, increases with the size of the island, eventually slowing the diffusion significantly and limiting the islands to a certain maximal size. This is consistent with our experimental observations.

4.3. Joining of Islands. The mechanism for islands joining together (Figure 2c) could be collisions of islands if they were mobile on the film, although the low number of doublets and absence of multiplets would suggest that is unlikely. Alternatively, the mechanism could be explained by neighboring islands growing until they collide with each other. It is noteworthy that after joining they remain as two circular islands in contact rather than coalescing into a single larger island. This observation does not seem consistent with an Ostwald ripening mechanism, which would allow one island to grow at the expense of the other.

The voids that appear in the film (Figure 2c) are generally associated with island doublets or a higher than average number of islands in the vicinity. This suggests that the mercury-rich material in the islands is consuming gold from the nearby film.

4.4. Development of Dendritic Structure with Neighboring Bare Strips in the Gold Film. Following formation of island doublets, their growth proceeds via a new mechanism—anisotropic dendritic growth. Dendritic structures are characteristic of diffusion-limited growth. In this case, we propose that gold from the film is being drawn into the mercury-rich islands, driven by concentration gradients and the tendency to make the amalgam concentration uniform throughout the features. After the formation of island doublets, the concentration gradient that drives the diffusion of mercury and gold from the film into the islands is greatest along a line drawn through the island centers and extended outside the islands. Diffusion then tends to deposit material along this axis, forming an elongated "finger" structure. The maximum concentration gradients remain at the tips of the fingers, so the tendency to produce long fingers or dendrites is sustained.

The dendrites each maintain a width of around 1 μm, but the "trees" that they form extend for tens of microns. This heterogeneous structure will scatter light strongly, accounting for the dull appearance to the naked eye of a film that has been exposed to mercury for several hours. The scattering of light also accounts for the reduction of reflectivity observed here (Figure 6e) and proposed by others as the basis for a mercury sensor.[11,13]

4.5. Final Threads-Plus Islands Structure. The final structure is discontinuous, as seen in Figure 2e. Previous authors have noted an increase in resistivity of gold films exposed to mercury[24,31] and have proposed this as a possible sensing method—the destruction of a continuous gold film is the obvious explanation for increased resistivity. This morphology change is also consistent with our FECO results (Figure 6e′). The fringe positions in the Au-coated domain of a half-coated wafer show an abrupt shift back to their positions in the bare SiO_2 domain, because bare SiO_2 surface is exposed and becomes the predominant reflective surface after the destruction of the Au film.

The morphological change from dendritic to discontinuous is reminiscent of spinodal dewetting,[28] and also of the Rayleigh instability in which a thread of liquid breaks into isolated drops. In either case, this suggests that Au—Hg amalgam behaves like a liquid, which does not wet the SiO_2/Si surface when all of the Au film has been consumed. Because the SiO_2 is already bare (devoid of gold) in the neighborhood of the dendritic structures, the dewetting does not appear to be an abrupt event and so the Rayleigh instability driven by the amalgam's surface tension seems a more likely explanation than spinodal dewetting. The liquid-like behavior of Au—Hg amalgam can be explained from the Au—Hg binary phase diagram,[44] in which liquid and solid phases coexist when the atomic percent of Hg is more than 34% at room temperature.

5. CONCLUSION

We have used SEM and AFM imaging to characterize the morphological evolution of mercury sorption on a thin polycrystalline gold film. Although many of the observed features have been reported in earlier literature, we are not aware of any previous attempt to explain the whole sequence of morphologies as we have done here. In the early stages of exposure to mercury vapor, mercury sorption results in surface reconstruction and displacement of gold atoms from the film, leading to the formation of pits in the gold film and mercury-rich islands. The islands grow to micrometer size with further arrival of mercury atoms and diffusion of gold into the islands that leaves voids in the gold film. Rather than indefinite growth in the size of circular islands, diffusion-limited growth leads to

DOI: 10.1021/acsami.5b07002
ACS Appl. Mater. Interfaces 2015, 7, 23172−23181

formation of dendritic structures with neighboring voids in the gold film. After prolonged exposure, the dendritic fingers appear to be sufficiently fluid that a Rayleigh instability occurs and the final structure is a set of small droplets.

With regard to mercury vapor sensor applications, the irreversible morphological changes render this type of film impractical for long-term monitoring of mercury vapor, although films formed from other gold structures such as nanoprisms show more promise in this regard.[48,49] In particular, the irregular fringe shifts observed in FECO measurements suggest it is unwise to use optical interferometry, ellipsometry or SPR techniques in the implementation of Au film-based devices because the film is attacked by mercury and becomes highly scattering. In addition, the reproducibility of results depends on detailed experimental conditions such as gold film thickness, adsorption rate, exposure time, and equilibration time. Furthermore, sorption in this stage is irreversible,[23] and there is evidence that the surface structure may change with time,[27,29] both of which may make the gold film unsuitable as a sensor for mercury vapor at high concentrations or long exposure times. Using a Cr layer to promote adhesion of a gold film to an insulating substrate inhibits the formation of pits and postpones the appearance of voids in the gold film, but the mercury still accumulates in micrometer-scale islands that would scatter light and make optical detection qualitative only.

AUTHOR INFORMATION

Corresponding Author

*E-mail: r.horn@deakin.edu.au.

Notes

The authors declare no competing financial interest.

ACKNOWLEDGMENTS

We thank Deakin University for financial support, including a PhD scholarship for T.H.. This work was performed in part at the Melbourne Centre for Nanofabrication (MCN) in the Victorian node of the Australian National Fabrication Facility (ANFF). We thank Dr. Yunfei Ding, Dr. Xiaodong She, and Dr. Andrew Sullivan for their assistance with SEM imaging; and Dr. Yang Lim (MCN) and Dr. Hemayet Uddin (MCN) for their assistance with Au film preparation and AFM imaging.

REFERENCES

(1) Carpi, A. Mercury from Combustion Sources: A Review of the Chemical Species Emitted and Their Transport in the Atmosphere. *Water, Air, Soil Pollut.* **1997**, *98*, 241−254.

(2) Driscoll, C. T.; Han, Y.-J.; Chen, C. Y.; Evers, D. C.; Lambert, K. F.; Holsen, T. M.; Kamman, N. C.; Munson, R. K. Mercury Contamination in Forest and Freshwater Ecosystems in the Northeastern United States. *BioScience* **2007**, *57*, 17−28.

(3) Schober, S. E.; Sinks, T. H.; Jones, R. L.; Bolger, P. M.; McDowell, M.; Osterloh, J.; Garrett, E. S.; Canady, R. A.; Dillon, C. F.; Sun, Y. Blood Mercury Levels in Us Children and Women of Childbearing Age, 1999−2000. *JAMA* **2003**, *289*, 1667−1674.

(4) Bloom, N.; Fitzgerald, W. F. Determination of Volatile Mercury Species at the Picogram Level by Low-Temperature Gas Chromatography with Cold-Vapour Atomic Fluorescence Detection. *Anal. Chim. Acta* **1988**, *208*, 151−161.

(5) Hatch, W. R.; Ott, W. L. Determination of Submicrogram Quantities of Mercury by Atomic Absorption Spectrophotometry. *Anal. Chem.* **1968**, *40*, 2085−2087.

(6) Bushee, D. S. Speciation of Mercury Using Liquid Chromatography with Detection by Inductively Coupled Plasma Mass Spectrometry. *Analyst* **1988**, *113*, 1167−1170.

(7) Amyot, M.; Gill, G. A.; Morel, F. M. Production and Loss of Dissolved Gaseous Mercury in Coastal Seawater. *Environ. Sci. Technol.* **1997**, *31*, 3606−3611.

(8) McNerney, J. J.; Buseck, P. R.; Hanson, R. C. Mercury Detection by Means of Thin Gold Films. *Science* **1972**, *178*, 611−612.

(9) Sabri, Y.; Kojima, R.; Ippolito, S.; Wlodarski, W.; Kalantar-Zadeh, K.; Kaner, R.; Bhargava, S. QCM Based Mercury Vapor Sensor Modified with Polypyrrole Supported Palladium. *Sens. Actuators, B* **2011**, *160*, 616−622.

(10) Sabri, Y.; Ippolito, S.; Tardio, J.; Atanacio, A.; Sood, D.; Bhargava, S. Mercury Diffusion in Gold and Silver Thin Film Electrodes on Quartz Crystal Microbalance Sensors. *Sens. Actuators, B* **2009**, *137*, 246−252.

(11) Butler, M. Mercury Adsorption on Optically Thin Gold Films. *J. Appl. Phys.* **1990**, *67*, 4320−4326.

(12) Morris, T.; Szulczewski, G. A Spectroscopic Ellipsometry, Surface Plasmon Resonance, and X-Ray Photoelectron Spectroscopy Study of Hg Adsorption on Gold Surfaces. *Langmuir* **2002**, *18*, 2260−2264.

(13) Morris, T.; Szulczewski, G. Evaluating the Role of Coinage Metal Films in the Detection of Mercury Vapor by Surface Plasmon Resonance Spectroscopy. *Langmuir* **2002**, *18*, 5823−5829.

(14) Wang, C.; Ma, Z.; Hossain, M.; Su, M. Visual Detection of Mercury Vapor Using Plasmonic Nanoparticle Array. In *9th Annual IEEE Conference on Sensors*; Waikoloa, HI, Nov 1−4, 2010 ; IEEE: Piscataway, NJ, 2010; pp 323−326.

(15) Scallan, K. F. Detection of Elemental Mercury by Gold Nanoparticles. *Ph.D Thesis*, University of California, Berkeley, CA, 2007.

(16) Morris, T.; Kloepper, K.; Wilson, S.; Szulczewski, G. A Spectroscopic Study of Mercury Vapor Adsorption on Gold Nanoparticle Films. *J. Colloid Interface Sci.* **2002**, *254*, 49−55.

(17) James, J. Z. Mercury Sensing with Optically Responsive Gold Nanoparticles. *Ph.D Thesis*, University of California, Berkeley, CA, 2012.

(18) Morris, T.; Copeland, H.; McLinden, E.; Wilson, S.; Szulczewski, G. The Effects of Mercury Adsorption on the Optical Response of Size-Selected Gold and Silver Nanoparticles. *Langmuir* **2002**, *18*, 7261−7264.

(19) Rex, M.; Hernandez, F. E.; Campiglia, A. D. Pushing the Limits of Mercury Sensors with Gold Nanorods. *Anal. Chem.* **2006**, *78*, 445−451.

(20) Chemnasiri, W.; Hernandez, F. E. Gold Nanorod-Based Mercury Sensor Using Functionalized Glass Substrates. *Sens. Actuators, B* **2012**, *173*, 322−328.

(21) James, J. Z.; Lucas, D.; Koshland, C. P. Gold Nanoparticle Films as Sensitive and Reusable Elemental Mercury Sensors. *Environ. Sci. Technol.* **2012**, *46*, 9557−9562.

(22) McNicholas, T. P.; Zhao, K.; Yang, C.; Hernandez, S. C.; Mulchandani, A.; Myung, N. V.; Deshusses, M. A. Sensitive Detection of Elemental Mercury Vapor by Gold-Nanoparticle-Decorated Carbon Nanotube Sensors. *J. Phys. Chem. C* **2011**, *115*, 13927−13931.

(23) Battistoni, C.; Bemporad, E.; Galdikas, A.; Kačiulis, S.; Mattogno, G.; Mickevičius, S.; Olevano, V. Interaction of Mercury Vapour with Thin Films of Gold. *Appl. Surf. Sci.* **1996**, *103*, 107−111.

(24) Adamov, M.; Perović, B.; Nenadović, T. Electrical and Structural Properties of Thin Gold Films Obtained by Vacuum Evaporation and Sputtering. *Thin Solid Films* **1974**, *24*, 89−100.

(25) George, M.; Glaunsinger, W. The Electrical and Structural Properties of Gold Films and Mercury-Covered Gold Films. *Thin Solid Films* **1994**, *245*, 215−224.

(26) Levlin, M.; Ikävalko, E.; Laitinen, T. Adsorption of Mercury on Gold and Silver Surfaces. *Fresenius' J. Anal. Chem.* **1999**, *365*, 577−586.

(27) Levlin, M.; Niemi, H.-M.; Hautojärvi, P.; Ikävalko, E.; Laitinen, T. Mercury Adsorption on Gold Surfaces Employed in the Sampling and Determination of Vaporous Mercury: A Scanning Tunneling Microscopy Study. *Fresenius' J. Anal. Chem.* **1996**, *355*, 2−9.

(28) Fialkowski, M.; Grzeszczak, P.; Nowakowski, R.; Holyst, R. Absorption of Mercury in Gold Films and Its Further Desorption:

DOI: 10.1021/acsami.5b07002
ACS Appl. Mater. Interfaces 2015, 7, 23172−23181

Quantitative Morphological Study of the Surface Patterns. *J. Phys. Chem. B* **2004**, *108*, 5026−5030.
(29) Nowakowski, R.; Kobiela, T.; Wolfram, Z.; Duś, R. Atomic Force Microscopy of Auhg Alloy Formation on Thin Au Films. *Appl. Surf. Sci.* **1997**, *115*, 217−231.
(30) Hariharan, P. *Optical Interferometry*, 2nd ed.; Academic Press: San Diego, 2003; p 351.
(31) George, M. A. Electrical, Spectroscopic and Morphological Investigation of Mercury Adsorption on Thin Gold Films. *Ph.D Thesis*, Arizona State University, Mesa, AZ, 1991.
(32) Nowakowski, R.; Pielaszek, J.; Duś, R. Surface Mediated Ag−Hg Alloy Formation under Ambient and Vacuum Conditions-Afm and Xrd Investigations. *Appl. Surf. Sci.* **2002**, *199*, 40−51.
(33) Born, M.; Wolf, E. *Principles of Optics: Electromagnetic Theory of Propagation, Interference and Diffraction of Light*, 6th ed.; Cambridge University Press: Cambridge, U.K., 1997; p 808.
(34) Clarkson, M. Multiple-Beam Interferometry with Thin Metal Films and Unsymmetrical Systems. *J. Phys. D: Appl. Phys.* **1989**, *22*, 475.
(35) Hirschorn, E.; Miller, T.; Sieger, M.; Chiang, T.-C. Atomic Exchange and Growth of Au on Ag (110). *Surf. Sci.* **1993**, *295*, L1045−L1049.
(36) Hirschorn, E.; Lin, D.; Hansen, E.; Chiang, T.-C. Atomic Burrowing and Hole Formation for Au Growth on Ag (110). *Surf. Sci.* **1995**, *323*, L299−L304.
(37) Poirier, G. Mechanism of Formation of Au Vacancy Islands in Alkanethiol Monolayers on Au (111). *Langmuir* **1997**, *13*, 2019−2026.
(38) Poirier, G. E. Characterization of Organosulfur Molecular Monolayers on Au (111) Using Scanning Tunneling Microscopy. *Chem. Rev.* **1997**, *97*, 1117−1128.
(39) Yang, G.; Liu, G.-y. New Insights for Self-Assembled Monolayers of Organothiols on Au (111) Revealed by Scanning Tunneling Microscopy. *J. Phys. Chem. B* **2003**, *107*, 8746−8759.
(40) Langmuir, I. The Constitution and Fundamental Properties of Solids and Liquids. Part I. Solids. *J. Am. Chem. Soc.* **1916**, *38*, 2221−2295.
(41) Besenbacher, F. Scanning Tunnelling Microscopy Studies of Metal Surfaces. *Rep. Prog. Phys.* **1996**, *59*, 1737.
(42) Heine, V.; Marks, L. Competition between Pairwise and Multi-Atom Forces at Noble Metal Surfaces. *Surf. Sci.* **1986**, *165*, 65−82.
(43) Trevor, D. J.; Chidsey, C. E.; Loiacono, D. N. In Situ Scanning-Tunneling-Microscope Observation of Roughening, Annealing, and Dissolution of Gold (111) in an Electrochemical Cell. *Phys. Rev. Lett.* **1989**, *62*, 209−212.
(44) Rolfe, C.; Hume-Rothery, W. The Constitution of Alloys of Gold and Mercury. *J. Less-Common Met.* **1967**, *13*, 1−10.
(45) Kita, H.; Kon, T. Hydrogen Evolution Reaction on Gold-Mercury Alloys of Various Conposition. *J. Res. Inst. Catalysis, Hokkaido Univ.* **1971**, *19*, 167−180.
(46) Chen, Y.; Washburn, J. Structural Transition in Large-Lattice-Mismatch Heteroepitaxy. *Phys. Rev. Lett.* **1996**, *77*, 4046−4049.
(47) Zinke-Allmang, M.; Feldman, L. C.; Nakahara, S. Role of Ostwald Ripening in Islanding Processes. *Appl. Phys. Lett.* **1987**, *51*, 975−977.
(48) Sabri, Y. M.; Ippolito, S. J.; Tardio, J.; Bansal, V.; O'Mullane, A. P.; Bhargava, S. K. Gold Nanospikes Based Microsensor as a Highly Accurate Mercury Emission Monitoring System. *Sci. Rep.* **2014**, *4*, 1−8.
(49) Sabri, Y.; Ippolito, S.; O'Mullane, A.; Tardio, J.; Bansal, V.; Bhargava, S. Creating Gold Nanoprisms Directly on Quartz Crystal Microbalance Electrodes for Mercury Vapor Sensing. *Nanotechnology* **2011**, *22*, 305501−305509.

DOI: 10.1021/acsami.5b07002
ACS Appl. Mater. Interfaces 2015, 7, 23172−23181